Research article

Characterization of Critical Determinants of ACE2-RBD Interaction

Emily E. F. Brown[1,2 †], Reza Rezaei[1,2 †], Taylor Jamieson[1,2†], Jaahnavi Dave[1,2†], Nikolas T. Martin[1,2], Ragunath Singaravelu[1,2], Mathieu J.F. Crupi[1,2], Stephen Boulton[1,2], Sarah Tucker[1,2], Jessie Duong[1,2], Joanna Poutou[1,2], Adrian Pelin[1,2], Hamed Yasavoli-Sharahi[4], Zaid Taha[1,2], Rozanne Arulanandam[1,2], Abera Surendran[1,2], Mina Ghahremani[3], Bradley Austin[1,2], Chantal Matar[4], Jean-Simon Diallo[1,2], John C. Bell [1,2], Carolina S. Ilkow [1,2], and Taha Azad [1,2]*

[1] Ottawa Hospital Research Institute, Ottawa, ON, K1H 8L6, Canada.

[2] Department of Biochemistry, Microbiology and Immunology, University of Ottawa, Ottawa, ON K1H 8M5, Canada.

[3] Department of Biology, University of Ottawa, Ottawa, ON, K1N 6N5, Canada.

[4] Cellular and Molecular Medicine Department, Faculty of Medicine, University of Ottawa, Canada

* Correspondence: tazad@ohri.ca; Tel.: +1-613-737-8899 (ext. 75208).

† These authors contributed equally.

Abstract

Despite sequence similarity to SARS-CoV-1, SARS-CoV-2 has demonstrated greater widespread virulence and unique challenges to researchers aiming to study its pathogenicity in humans. The interaction of the viral receptor binding domain (RBD) with its main host cell receptor, angiotensin-converting enzyme 2 (ACE2), has emerged as a critical focal point for the development of anti-viral therapeutics and vaccines. Utilizing our recently developed NanoBiT technology-based biosensor, we selectively identify and characterize the impact of mutating certain amino acid residues in the RBD of SARS-CoV-2 and in ACE2. Specifically, we examine the mutational effects on RBD-ACE2 binding ability, before and after the addition of competitive inhibitors, as well as neutralizing antibody activity. These critical determinants of virus-host interactions may provide more effective targets for ongoing vaccines, drug development, and potentially pave the way for determining the genetic variation underlying disease severity.

Keywords: SARS-CoV-2; angiotensin-converting enzyme 2; receptor binding domain; NanoLuc Binary Technology; spike protein; vaccine development, drug development, bioluminescence

1. Introduction

The severe acute respiratory syndrome coronavirus 2 (SARS-CoV-2) is the etiologic agent responsible for the COVID-19 pandemic and is an ongoing worldwide public health threat. As of October 16th 2020, there have been over 39 million confirmed cases, and over 1 million confirmed deaths resulting from SARS-CoV-2 infection (WHO reports, https://www.who.int/emergencies/diseases/novel-coronavirus-2019/situation-reports). Tremendous efforts are currently underway to develop rapid drug screening methodologies and novel vaccines. The large variability of disease severity among individuals infected with SARS-CoV-2 continues to be investigated [1] and new findings in this field may shed light on strategies to tailor these new therapeutics to patients.

Entry of SARS-CoV-2 is mediated by interaction of the viral Spike glycoprotein (S) with its main target receptor angiotensin converting enzyme 2 (ACE2), found on the surface of mammalian cells, primarily in the lower respiratory tract [2]. The S protein is composed of two subunits, S1 and S2, which play cooperatively a role in viral entry and fusion of the viral membrane with host cell membrane. Binding to ACE2 is mediated by the receptor binding domain (RBD), located in the C-terminus of the S1 subunit [3]. The identification of amino acid residues that are crucial for the interaction of RBD with ACE2 is of great interest to gain a better understanding of the interplay between viral entry and host genetic factors which may contribute to the observed variability in disease pathogenesis. As such, characterizing functional mutants of RBD and ACE2 may provide critical insights for the development of drugs and vaccines.

The development of biosensor technology is a highly valuable and sensitive analytical tool with a broad spectrum of applications, such as diagnosis and drug development [4, 5]. Biosensors designed to emit bioluminescence often rely on luciferase, a class of enzymes that catalyze substrate to produce a bioluminescent signal. One such tool is the NanoLuc Binary Technology (NanoBiT), which enables rapid analysis of protein-protein interactions through use of Nanoluciferase, a small luciferase reporter [5-12]. By exploiting this technology, we have recently developed an assay to rapidly investigate RBD and ACE2 interactions. In addition, this assay can be used to elucidate the impact of both RBD and ACE2 amino acid mutations on their binding abilities, as well as their potential implications for drug development and evaluating immune responses.

Previous studies have examined crucial residues in ACE2 and the SARS-CoV-1 Spike domain [13, 14]. Similarly, recent studies have begun to unravel important interactions in SARS-CoV-2 RBD and ACE2 [15]. While some progress has been made towards examining the impact of specific mutations within the SARS-CoV-2 RBD and ACE2, there remain much to be studied with regards to their impact on binding, infectivity and host susceptibility to viral infection. In addition, the impact of specific RBD mutations on the efficacy of potential therapeutics has not been explored. For example, most vaccines under development are designed to contain the RBD domain of S, and sequencing data has shown that RBD is among the most non-conservative domain in SARS-CoV-2 S [16]. Thus, the question that still remain is whether SARS-CoV-2 viruses harboring select RBD mutations would be controlled by immune responses mounted against the RBD sequence encoded in the original virus strain. Another unexplored area is whether variations in host ACE2 sequences could alter virus susceptibility and/or disease severity among individuals or species. Comparisons on how mutations in ACE2 affect binding of the RBD from SARS-CoV-1 versus SARS-CoV-2 have yet to be performed. We believe that elucidating which variations may have an impact in the ACE2: SARS-CoV-2 S binding affinity is worth investigating since this information could impact the development of therapeutic options for COVID-19 patients. Here, we investigate whether any of these critical amino acid sites in ACE2 exist in the human population and may explain severity of the disease.

2. Results and Discussion

The first crucial step of SARS-CoV-2 viral entry is mediated by binding of RBD to ACE2, its main cognate receptor expressed on the surface of the human airway epithelium (**Figure 1A**). In this study, we aim to investigate whether selected mutations in both SARS-CoV-2 S protein RBD and its host receptor ACE2 could impact their interactions with one another. We also examine how specific mutations in ACE and RBD may alter the efficacy of drugs and neutralizing antibodies being developed for treatment and disease prevention purposes, respectively. To accomplish these aims, we use a NanoBiT SARS-CoV-2-RBD and ACE2 biosensor, previously developed by our lab, to initially characterize the RBD: ACE2 interaction (**Figure 1B**) [17]. The molecular basis of this technology involves the fusion of a Large Bit (LgBiT) subunit to one of the proteins of interest, and the fusion of a Small Bit subunit (SmBiT) to the second protein being investigated. As illustrated in **Figure 1B**, LgBiT and SmBiT alone have poor affinity for one

another; however, both subunits interact to produce a bioluminescent signal in the presence of furimazine, the substrate for Nanoluciferase, if the fusion proteins interact with each other.

Mutations within the ACE2 ectodomain alter binding affinity of ACE2 with SARS-CoV-2 RBD, SARS-CoV-2 S1 subunit, and SARS-CoV-1 RBD

ACE2 is a key interacting partner involved in SARS-CoV-2 viral entry, thus we first performed *in silico* mutagenesis analysis to assess putative ACE2 mutants that could be potentially defective at interacting with SARS-CoV-2 RBD. Based on the overall 3D crystal structure analysis of ACE2 bound to RBD (**Figure 2A, B**), we selectively identified 22 sites in ACE2, which are most likely involved in ACE: RBD direct interaction (**Figure 2** A-D). To analyze the contribution of these 22 mutants on their ability to interact with RBD using our NanoBiT based biosensor technology, we first engineered the 22 amino acid mutants of ACE2 (**Figure 2E**) and linked them to SmBiT. Expression of ACE2 mutants from transfected HEK293T cells was demonstrated by immunoblotting (**Figure 3A**).

We then investigated the binding affinity of ACE2 wild-type and mutants with both SARS-CoV-2-RBD and SARS-CoV-2 S1 as complementary binding partner. The rationale for also including an S1-based NanoBiT binding partner in our assays was that RBD is encompassed within the S1 subunit of the S glycoprotein. Hence, including S1 would more closely mimic SARS-CoV-2 S behavior in the context of viral infection. Thus, we proceeded to compare whether S1 fused to LgBiT and RBD-LgBiT constructs have similar binding affinity for ACE and its mutants. When combined with SARS-CoV-2-RBD-LgBiT, 12 of the 22 mutants of ACE2 showed a significant decrease in their binding affinity (**Figure 3B**). Specifically, ACE2 mutants Q24A, F28A, D38A, Y41A, K353A, G354D, D355A, R357A, and NFS (residues 82-84) demonstrated reduced binding to SARS-CoV-2-RBD (**Figure 3B**). We also found that 13 of the 22 mutants showed a significant decrease in binding to S1 (**Figure 3C**). Specifically, ACE2 mutants Q24A, F28A, D38A, Y41A, Q42A, L45A, M82A, Y83A, K353A, G354D, D355A, R357A, and NFS had reduced binding to SARS-CoV-2 S1 (**Figure 3C**). In summary, we found that the same 12 ACE2 mutants that showed decreased binding to SARS CoV-2 RBD also has impaired interactions with SARS CoV-2 S1, with the addition of mutant Y83A that reported a reduced affinity for SARS-CoV-1 S1 only.

Since structural analysis has shown that certain residues in SARS-CoV-2 RBD are well conserved within SARS-CoV-1 RBD [17], we decided to also combined the various ACE2-SmBiT mutants with a LgBiT-SARS-CoV-1 RBD construct. This allowed us to also evaluate how ACE2 mutations could impact ACE2 : SARS-CoV-1 RBD interaction. In figure 3D, we further show that 14 different ACE2 mutations (T27D, F28A, H34A, E35A, E37A, Y41A, Q42A, L45A, Y83A, K353A, G354D, D355A, R357A, and NFS) significantly alter its respective binding efficiency to the wild type SARS-CoV-1 RBD. Of note, ten of these ACE2 mutants are in common with SARS-CoV-2 RBD. These data suggest that in comparison with SARS-CoV-1 RBD, SARS-CoV-2 RBD may be slightly more resistant to ACE2 mutants, which may arise from single nucleotide polymorphisms (SNPs). This observation may have implications with regards to viral susceptibility of various species or individuals based on their ACE2 gene sequence.

SARS-CoV-2 Spike pseudotyped lentiviral particle assay confirm that mutations within the ACE2 ectodomain alter binding affinity of ACE2 with SARS-CoV-2 RBD

To reinforce the ACE2 mutational findings observed with our biosensor technology described above, we then decided to utilize a lentiviral-based pseudovirus infectivity assay. We hypothetized that ACE2 mutants which retain their binding capacity to SARS-CoV-2 RBD should act as competitive inhibitors for SARS-CoV-2 pseudovirus binding to ACE2 in the host cell, and thus reducing its infectivity (**Figure 4A**). To test this notion, we combined each of the 22 ACE2 mutants with SARS-CoV-2 spike pseudotyped lentivirus expressing luciferase, and then added the pre-treated pseudovirus samples to HEK293X cells expressing ACE2 and TMPRSS2 (the host protease responsible for cleaving S glycoprotein[18]). We then measured the infectivity with a luciferase assay - a lower signal is indicative of reduced infection, resulting from ACE2 mutants retaining RBD binding capacity, thereby acting as competitive inhibitors (**Figure 4B**). These results very closely align with mutant binding affinity changes observed with our biosensor technology (**Figure 3B-C**).

Utilizing ACE2 sequences as a predictor for the SARS-CoV-2 susceptibility of various species and mutation prevalence in humans

Our findings suggest that identification of ACE2 amino acid sites which impact RBD binding may provide insights as to SARS-CoV-2 susceptibilities of different individuals or species

based on their genetics. Using multiple sequence alignments of the 12 target mutation sites identified to be essential for RBD binding (**Figure 3**), we propose a method to predict SARS-CoV-2 virus susceptibility (**Figure 5A**). It is plausible to hypothetize that any species with an identical ACE2 amino acid sequence to the human ACE2 receptor would theoretically be highly susceptible to the virus, and possibly act as a source of transmission, such as the common chimpanzee (*Pan troglodytes*; **Figure 5A**). With the presence of only one or two differences at key ACE2 binding sites, it is likely that species such as *Tursiops truncatus* (bottlenose dolphin) or *Cricetulus griseus* (Chinese hamster) would still be infected by SARS-CoV-2. In contrast, species such as domesticated horses (*Equus caballus*) or brown rats (*Rattus norvegicus*), which have many differences at key ACE2 residues, are expected to be less susceptible to SARS-CoV-2 infection, due to reduced binding efficiency between ACE2 and RBD. With reduced binding efficacy, viral infection and spread would likely be impaired in these animals, leading them to pose less of a risk for shedding large amounts of infectious virus potentially leading to reduced viral pathogenesis (**Figure 5A**). These findings are consistent with literature studies of optimal SARS-CoV-2 disease models [19]. For example, increasing studies have indicated that hamsters are a better suited animal model to study SARS-CoV-2 in comparison to mice [20].

Looking at the prevalence of these mutations in people, we observe that some of these SNPs (namely NFS, G354, and D355) already exist in a small fraction of the population (**Figure 5B**). Our data suggest the possibility that individuals harboring these SNPs may be more resistant to the SARS-CoV-2 virus infection. Genetic differences in the ACE2 receptor of individuals may also provide a partial explanation for the variability in disease severity among individuals. Interestingly, *in silico* studies from other groups have also suggested that genetic influences cause interindividual variability in ACE2 expression [21], [22]. In this study, we experimentally validated for the first time the effects of ACE2 mutants on RBD binding affinity, which may pave the path for clinical studies.

Mutations in SARS-CoV-2 RBD that alter its ability to bind to ACE2 do not impact the activity of a competitive inhibitor nor the efficacy of a neutralizing antibody

A key concern surrounding RNA viruses, and viruses in general, is their capacity to evolve through the accumulation of mutations. Such mutations may drive resistance to therapeutics and/or evasion of host immune responses acquired through infection or vaccination against the wild-type virus. Recently two mutations in the SARS-CoV-2 RBD have been reported in Africa and the UK. We have investigated one of the critical mutation sites reported by the UK, asparagine residue at location 501 (N501), by altering the residue to both to Alanine and Tyrosine *in silico* (Figure 6 A-D). The change to alanine preserved the internal interactions of the residue with two glutamine residues at positions 498 and 506 but abolished the interaction with tyrosine 41 in ACE2. However, mutation to the tyrosine variant preserved all internal interactions and slightly strengthened them. Moreover, this mutation introduced a new strong interaction site, 2.3 A, with lysine 353 in ACE2 structure. Another recently discovered mutation is the change of glutamic acid at position 484 to lysine. We did not detect any significant change in internal or RBD-ACE2 interaction sites which may be due to the fact that this residue is located in a very flexible loop structure (Figure 6E-F).

Additionaly, we selected 16 of the 25 RBD mutants used in our recent study which retained some level of ACE2 binding capacity to further assess the effects of a competitive inhibitor and a neutralizing antibody with our biosensor assay. From a therapeutic perspective, recombinant RBD is under clinical consideration for use as a potential viral attachment inhibitor, given its ability to competitively inhibit SARS-CoV-2 virus particles [24]. We found that recombinant RBD expressed from mammalian cells wascapable of out-competing all 16 of the RBD mutants tested(Figure 6I). These results suggest that competitive drugs developed to combat the wild-type virus are still applicable to virus strains which may acquire these mutations in the RBD domain leading to reduced receptor binding over time. Neutralizing antibodies (nAb) play a key role in generating protective immunity against viral agents, and are developed through exposure to the virus itself, or to viral antigens in the form of a vaccine. We found that addition of a nAb significantly decreased, if not abolished, the interaction between all examined RBD mutants and ACE2 (Figure 6J). Importantly, this data may indicate that these receptor binding mutations do not provide an immune evasive advantage to the virus, and as a result, should not pose a serious threat to the efficacy of developed vaccines, and immunity, to viruses harboring these mutations.

Conservation of RBD across coronavirus strains

We used multiple sequence alignment tools to further investigate amino acid conservation patterns of the RBD mutants under examination across multiple betacoronavirus strains. This analysis could provide interesting insights on the possible contributions of these specific residues in RBD and their link to infectivity. The variation in amino acid sites is indicative of which amino acids are critical for maintaining the structural integrity of RBD, and which can be modified for therapeutic purposes. For example, amino acid C361 is present in the bottom of the RBD core, and not at the contact site. Considering the cross-species conservation of this residue, it may exert an important role in stabilizing the overall structure of the protein. Of the analyzed amino acids, K417 was the only one which was not part of RBM, yet is still in close proximity to the contact site, providing important contact with residue D30 in the ACE2 structure [3]. Of the other Betacoronavirus species analyzed in this study, the presence of K417 is limited to SARS-CoV-2. This unique event could be aone of the possible reason for which SARS-CoV-2 exhibits a higher binding efficiency to ACE2 compared to other viruses in the same family. It is also likely to expect that Betacoronaviruses harboring low amino acid sequence similarity to SARS-CoV-2 likely utilize a different host receptor for viral entry. In addition, when analyzing tyrosine residues at positionY449 and Y505, it seems that the hydroxyl (OH) group in the tyrosine side chain may possibly contact two different amino acids on ACE2 structure, appearing critical for effective binding of the receptor-ligand structure. Precisely, Y449 contacts D38 and Q42 in ACE2, and Y505 contacts E37 and R393 in ACE2, respectively [3].

Elucidating which amino acids are conserved and occupy critical roles in viral ligand-host receptor binding could deepen our understanding of antiviral drug development. To increase the spectrum of antiviral agents directed towards betacoronaviruses, targeting conserved amino acids which are crucial for receptor binding may prove to be an interesting strategy. Given the conservation of amino acids between SARS-CoV-2, SARS-CoV-1 and MERS, it would be of interest to develop a therapeutics targeting this triad of viruses.

It has been theorized that the SARS-CoV-2 virus originated from bats, was then transmitted to pangolins, and finally spilled over to humans [25], [26], [27]. We examined the conservation of the 25 RBD point mutants generated in our study to determine if variations in amino acid sequence would follow the predicted path of interspecies transmission. Interestingly, these sites were mostly

conserved across all three species, with only three sites (V445, F486, and Y505) differing in bat CoV, when compared to pangolin Co-V and human SARS-CoV-2, and only one site (K417) differing in pangolin CoV compared to the bat and human viruses (Figure 7). These observations are in line with a recent report by Liu *et al.* [27]. In this study, the authors aligned the full-length spike sequence of SARS-CoV-2, Pangolin-CoV and Bat-CoV-RaTG13. These results and our predictions reported herein support the hypothesis that the path of viral transmission originated from bats, continued to pangolins as intermediate hosts, and then followed its dispersal route to the human population.

3. Conclusions

In this study, we provide for the first time a comprehensive overview of the effects of select mutations in both the ectodomain of ACE2 and the RBD of SARS-CoV-2. Our findings suggest that ACE2 SNPs in the human population may account for the variability in infectivity and disease progression in the context of SARS-CoV-2 infection. Furthermore, our observations from RBD mutational scanning also provide potential sites for drug targeting and therapeutic development. By combining ACE2 and RBD mutational analyses, we provide insights into the genetics underlying virus susceptibility and the development of possible therapeutic targets.

4. Materials and Methods

4.1. Cell lines

HEK293T (ATCC® CRL-3216) human embryonic kidney cells were obtained from ATCC. Cells were maintained in Dulbecco's Modified Eagle's Medium (Gibco), supplemented with 10% FBS (VWR) and 1% penicillin/streptomycin (Invitrogen). Cells were incubated in a humidified 37^0C incubator at 5% CO_2. Cells are routinely tested for mycoplasma by PCR testing, and used for up to 20 passages after thawing.

4.2. Plasmids

Engineered inserts are outlined in Supplementary Table 1 (GenScript). All biosensor subunits were cloned into the BamHI/NotI sites of pcDNA3.1 to generate mammalian expression constructs.

4.3. Transient transfection

HEK293T cells were grown in 100 mm or 150 mm cell culture dishes to 70% confluence. Cells were transfected with 10 µg of DNA using PolyJet (SignaGen) according to manufacturer's protocol. 48 hours post-transfection, cell supernatants or cell lysates were harvested for subsequent testing.

4.4. In vitro NanoBit assay

293T cells were lysed using passive lysis buffer (Promega). NanoBiT assays were performed using native coelenterazine (CTZ; 3.33 mM final concentration; Nanolight Technologies – Prolume Ltd., Pinetop, AZ, USA). Synergy Microplate Reader (BioTek, Winooski, VT, USA) was used to measure luminescence. Results are presented as raw RLU (Relative Luminescence Unit), or normalized to control where indicated. The data presented are the mean of three biological replicates.

4.5. Western immunoblotting

293T cells were lysed using passive lysis buffer. Protein concentration in clarified whole cell lysates was quantified using bicinchoninic acid assay (BCA) (Pierce). 20 µg of total protein was prepared in 1x Laemmli buffer, loaded into 4-12% gradient Bis-Tris acrylamide gels and resolved. Following transfer onto nitrocellulose membrane, blots were incubated in 0.1% Ponceau S solution (in 5% v/v acetic acid-distilled water) for 5 minutes at room temperature, imaged, then washed with TBST for 10 minutes. Blots were then blocked using 5% skimed milk powder in TBST for 1 hour. Blots were subsequently probed using anti-beta-actin primary antibody (1:5000), anti-HA tag (1:1000), or anti-FLAG tag (1:1000) in 5% milk overnight at 4˚C. Following washing with TBST, membranes were probed with HRP-conjugated secondary antibodies (1:10000) in 5% milk at room temperature for 1 hour. Blots were washed with TBST, then developed using BioRad Clarity-Western ECL and the BioRad ChemiDoc imaging system.

4.6. Lentiviral Pseudovirus Assay

Plasmid encoding SARS-CoV-2 spike pseudotyped lentivirus was kindly provided by Dr. Jesse Bloom (Fred Hutchinson Cancer Research Center, Seattle, WA) and lentivirus was generated as previously described (Crawford et. al., 2020). HEK293T cells were seeded in 6 wells plates to 70% confluency and were transfected with 1ug of individual smBiT ACE2 mutant DNA using

PolyJet (SignaGen) according to manufacturer's protocol. 48 hours post-transfection, supernatants of transfected cells were harvested. Pseudotyped lentiviruses were incubated with each of the smBiT-ACE2 mutant containing supernatants for 1 hour at 37˚C. Immediately following the incubation period, polyclonal HEK293X cells stably overexpressing ACE2 and TMPRSS2 were transduced in 96 well format (300 000 cells). 4 hours post-transduction all media was replaced. 48 hours post-transduction, cells were lysed using 1X PLB, cell lysates were transferred to an opaque 96-well plate, and infection efficiency was measured by luciferase assay using the Bright-Glo Luciferase Assay system following manufacturer's protocols (Promega).

4.7. Statistical analysis

All graphs and statistical analyses were generated in Excel or GraphPad Prism v.8. Means of two groups were compared using two-tailed unpaired Student's t-test. Means of more than two groups were compared by one-way ANOVA with Dunnett's or Tukey's multiple comparisons correction. Alpha levels for all tests were 0.05, with a 95% confidence interval. Error is graphed as the standard deviation (SD). Measurements were taken from distinct samples (biological replicates). For all analyses, *P<0.05, **P<0.01, ***P<0.005, n.s. = not significant.

4.8. Multiple Sequence Alignment of ACE2 and Spike Sequences, and finding ACE2 SNPs in the target positions

All of the represented sequences were retrieved from NCBI refseq protein database. Multiple sequence alignment (MSA) was performed using Clustal Omega (Madeira et.al., 2019) algorithm with default parameters. Alignments were visualized and prepared for illustration using Jalview software (Waterhouse et.al., 2009). The multiple sequence alignment of ACE2 polypeptides was reordered based on the binding efficiency data in the J. Damas et al (Damas et.al., 2020). The NCBI dbSNP database was searched for possible single nucleotide polymorphisms (SNPs) in target mutation sites and the related information were gathered in a table using Microsoft Excel.

Funding:

The authors disclosed receipt of the following financial support for the research, authorship, and/or publication of this article: This work was funded by the generous support from the Ottawa Hospital Foundation and a grant from the Canadian Institutes of Health Research (#448323) to

J.C.B., C.S.I. and J-S.D. This work was also supported by a Fast Grant for COVID-19 Science to J.C.B. and C.S.I. as well as an Ontario Together Grant to J-S-D. T.A. is funded by a CIHR Banting Fellowship. R.S. is funded by a CIHR postdoctoral fellowship and a cluster MITACs fellowship. T.R.J. is funded by a CIHR Frederick Banting and Charles Best Canada and Graduate Scholarship and an Ontario Graduate Scholarship. E.E.F.B. is funded by a CIHR Frederick Banting and Charles Best Canada Graduate Scholarship and a Lebovic Fellowship. A.S. and S.T. were supported by NSERC Graduate Scholarships. M.J.F.C., J.D., S.B., N.T.M., J.P., J.T.W, J.D. and S.T. are funded by cluster MITACs fellowships. Finally, we would like to thank the excellent technical assistance of Xiaohong He, Ricardo Marius, Julia Petryk and Christiano Tanese De Souza.

Conflicts of Interest: The authors declare no conflict of interest

Supplemental Table 1

Insert	DNA sequence	Amino Acid sequence
SmBiT-ACE2	ATGTGCCCCCAAAAGTTGACCATCTC ATGGTTCGCAATTGTACTACTAGTGA GTCCCTTGATGGCAGGCGGAAGTGGA	MCPQKLTIS WFAIVLLVS PLMAGGSG

(IL12 secretion signal-ACE2-HA-His)	GGTTCCTCTGGAGTGACCGGATACAG	GSSGVTGYR
	GCTGTTCGAGGAGATCCTGCAGAGCA	LFEEILQSTIE
	CAATCGAGGAGCAGGCCAAGACCTT	EQAKTFLDK
	CCTGGACAAGTTTAACCACGAGGCCG	FNHEAEDLF
	AGGATCTGTTTTATCAGAGCTCCCTG	YQSSLASWN
	GCCTCCTGGAACTACAATACCAACAT	YNTNITEEN
	CACAGAGGAGAATGTGCAGAACATG	VQNMNNAG
	AACAATGCCGGCGACAAGTGGTCTGC	DKWSAFLKE
	CTTCCTGAAGGAGCAGAGCACACTGG	QSTLAQMYP
	CCCAGATGTACCCTCTGCAGGAGATC	LQEIQNLTV
	CAGAACCTGACCGTGAAGCTGCAGCT	KLQLQALQQ
	GCAGGCCCTGCAGCAGAATGGCTCTA	NGSSVLSED
	GCGTGCTGTCCGAGGATAAGTCTAAG	KSKRLNTIL
	CGGCTGAATACAATCCTGAACACCAT	NTMSTIYST
	GAGCACAATCTATTCCACCGGCAAGG	GKVCNPDNP
	TGTGCAATCCCGACAACCCTCAGGAG	QECLLLEPG
	TGTCTGCTGCTGGAGCCTGGCCTGAA	LNEIMANSL
	TGAGATCATGGCCAACAGCCTGGATT	DYNERLWA
	ACAATGAGAGGCTGTGGGCATGGGA	WESWRSEV
	GTCCTGGCGCTCTGAAGTGGGCAAGC	GKQLRPLYE
	AGCTGCGGCCACTGTACGAGGAGTAT	EYVVLKNE
	GTGGTGCTGAAGAACGAGATGGCCA	MARANHYE
	GAGCCAATCACTACGAGGACTATGGC	DYGDYWRG
	GATTACTGGAGGGGCGACTATGAGGT	DYEVNGVD
	GAACGGCGTGGACGGCTACGATTATA	GYDYSRGQL
	GCCGCGGCCAGCTGATCGAGGATGTG	IEDVEHTFEE
	GAGCACACATTCGAGGAGATCAAGC	IKPLYEHLH
	CCCTGTATGAGCACCTGCACGCCTAC	AYVRAKLM
	GTGCGGGCCAAGCTGATGAATGCCTA	NAYPSYISPI
	TCCAAGCTACATCTCCCCAATCGGAT	GCLPAHLLG
	GCCTGCCTGCACACCTGCTGGGCGAC	DMWGRFWT

	ATGTGGGGCAGATTCTGGACAAACCT	NLYSLTVPF
	GTACTCCCTGACCGTGCCATTTGGCC	GQKPNIDVT
	AGAAGCCCAATATCGACGTGACCGAT	DAMVDQAW
	GCCATGGTGGACCAGGCCTGGGATGC	DAQRIFKEA
	CCAGAGGATCTTCAAGGAGGCCGAG	EKFFVSVGL
	AAGTTCTTCGTGAGCGTGGGCCTGCC	PNMTQGFW
	AAACATGACACAGGGCTTTTGGGAG	ENSMLTDPG
	AATAGCATGCTGACCGACCCAGGCA	NVQKAVCH
	ACGTGCAGAAGGCCGTGTGCCACCCA	PTAWDLGK
	ACAGCATGGGACCTGGGCAAGGGCG	GDFRILMCT
	ATTTCCGCATCCTGATGTGCACCAAG	KVTMDDFLT
	GTGACAATGGACGATTTTCTGACCGC	AHHEMGHIQ
	CCACCACGAGATGGGCCACATCCAGT	YDMAYAAQ
	ATGATATGGCATACGCAGCACAGCCC	PFLLRNGAN
	TTCCTGCTGAGGAATGGCGCCAACGA	EGFHEAVGE
	GGGCTTTCACGAGGCCGTGGGCGAG	IMSLSAATP
	ATCATGTCTCTGAGCGCCGCCACACC	KHLKSIGLLS
	TAAGCACCTGAAGAGCATCGGCCTGC	PDFQEDNET
	TGTCCCCAGACTTCCAGGAGGATAAC	EINFLLKQA
	GAGACCGAGATCAATTTTCTGCTGAA	LTIVGTLPFT
	GCAGGCCCTGACCATCGTGGGCACAC	YMLEKWRW
	TGCCCTTCACCTATATGCTGGAGAAG	MVFKGEIPK
	TGGCGCTGGATGGTGTTTAAGGGCGA	DQWMKKW
	GATCCCTAAGGACCAGTGGATGAAG	WEMKREIV
	AAGTGGTGGGAGATGAAGCGGGAGA	GVVEPVPHD
	TCGTGGGCGTGGTGGAGCCTGTGCCA	ETYCDPASL
	CACGACGAGACCTACTGTGATCCTGC	FHVSNDYSFI
	CAGCCTGTTCCACGTGTCTAACGACT	RYYTRTLYQ
	ATAGCTTTATCAGGTACTATACCCGC	FQFQEALCQ
	ACACTGTACCAGTTCCAGTTTCAGGA	AAKHEGPLH
	GGCCCTGTGCCAGGCAGCAAAGCAC	KCDISNSTE

	GAGGGCCCACTGCACAAGTGTGATAT	AGQKLFNM
	CTCCAACTCTACAGAGGCCGGCCAGA	LRLGKSEPW
	AGCTGTTCAATATGCTGAGACTGGGC	TLALENVVG
	AAGTCCGAGCCATGGACCCTGGCCCT	AKNMNVRP
	GGAGAACGTGGTGGGAGCCAAGAAT	LLNYFEPLFT
	ATGAACGTGAGGCCTCTGCTGAATTA	WLKDQNKN
	TTTCGAGCCACTGTTTACATGGCTGA	SFVGWSTD
	AGGACCAGAATAAGAACTCCTTTGTG	WSPYADQSI
	GGCTGGTCCACCGACTGGTCTCCATA	KVRISLKSA
	CGCCGATCAGTCTATCAAGGTGAGGA	LGDKAYEW
	TCTCTCTGAAGAGCGCCCTGGGCGAC	NDNEMYLF
	AAGGCCTATGAGTGGAATGATAACG	RSSVAYAM
	AGATGTACCTGTTCAGATCCTCTGTG	RQYFLKVKN
	GCCTATGCCATGAGGCAGTACTTCCT	QMILFGEED
	GAAGGTGAAGAACCAGATGATCCTG	VRVANLKPR
	TTTGGCGAGGAGGACGTGCGGGTGG	ISFNFFVTAP
	CCAATCTGAAGCCCAGAATCAGCTTT	KNVSDIIPRT
	AACTTCTTTGTGACAGCCCCCAAGAA	EVEKAIRMS
	CGTGAGCGATATCATCCCTCGCACCG	RSRINDAFR
	AGGTGGAGAAGGCCATCCGGATGAG	LNDNSLEFL
	CCGGTCCAGAATCAACGACGCCTTCA	GIQPTLGPPN
	GACTGAATGATAACAGCCTGGAGTTT	QPPVSGSGY
	CTGGGCATCCAGCCTACCCTGGGACC	PYDVPDYAY
	ACCTAATCAGCCACCCGTGTCTGGCA	PYDVPDYAY
	GCGGCTACCCATATGACGTGCCCGAT	PYDVPDYAS
	TACGCCTATCCTTACGACGTGCCAGA	SGHIEGRHM
	TTATGCCTACCCCTATGACGTGCCTG	LEMGHHHH
	ATTACGCAAGCTCCGGACACATCGAG	HHHHHH
	GGCAGGCACATGCTGGAGATGGGCC	

	ATCATCACCATCATCACCACCACCAC CACTGA	
RBD-LgBiT (IgK leader-3XFLAG-RBD-LgBiT-His)	ATGGAGACAGACACACTCCTGCTATG	METDTLLL
	GGTACTGCTGCTCTGGGTTCCAGGTT	WVLLLWVP
	CCACTGGTGACTCTGGCTCTAGCGGC	GSTGDSGSS
	TCTGGCAGCGGCGACTACAAGGACC	GSGSGDYKD
	ACGACGGTGACTACAAGGACCACGA	HDGDYKDH
	CATCGACTACAAGGACGACGACGAC	DIDYKDDDD
	AAGGGAGGAGGAGGCTCTAGCGGCG	KGGGGSSGG
	GCAACATCACAAATCTGTGCCCATTC	NITNLCPFGE
	GGCGAGGTGTTTAACGCCACCAGATT	VFNATRFAS
	TGCCAGCGTGTATGCCTGGAACCGGA	VYAWNRKR
	AGAGAATCTCTAATTGCGTGGCCGAC	ISNCVADYS
	TATAGCGTGCTGTACAATAGCGCCTC	VLYNSASFS
	CTTCTCTACCTTTAAGTGCTATGGCGT	TFKCYGVSP
	GTCCCCCACAAAGCTGAACGACCTGT	TKLNDLCFT
	GCTTCACCAACGTGTACGCCGACTCT	NVYADSFVI
	TTTGTGATCAGGGGCGATGAGGTGCG	RGDEVRQIA
	CCAGATCGCACCTGGACAGACAGGC	PGQTGKIAD
	AAGATCGCCGACTACAACTATAAGCT	YNYKLPDDF
	GCCAGACGATTTCACCGGCTGCGTGA	TGCVIAWNS
	TCGCCTGGAATAGCAACAATCTGGAT	NNLDSKVG
	TCCAAAGTGGGCGGCAACTACAATTA	GNYNYLYR
	TCTGTACCGGCTGTTCAGAAAGAGCA	LFRKSNLKP
	ACCTGAAGCCCTTTGAGCGGGATATC	FERDISTEIY
	AGCACAGAGATCTACCAGGCAGGCT	QAGSTPCNG
	CCACCCCTTGCAACGGAGTGGAGGGC	VEGFNCYFP
	TTCAATTGTTATTTTCCCCTGCAGAGC	LQSYGFQPT
	TACGGCTTCCAGCCTACAAATGGCGT	NGVGYQPY
	GGGCTATCAGCCATACAGGGTGGTGG	RVVVLSFEL

	TGCTGTCCTTTGAGCTGCTGCACGCA	LHAPATVGS
	CCTGCAACCGTGGGGAGTTCCGGTGG	SGGGGSGGG
	TGGCGGGAGCGGAGGTGGAGGCTCG	GSSGGVFTL
	AGCGGTGGAGTGTTCACACTGGAGG	EDFVGDWE
	ACTTTGTGGGCGATTGGGAGCAGACC	QTAAYNLD
	GCCGCCTACAACCTGGACCAGGTGCT	QVLEQGGVS
	GGAGCAGGGAGGCGTGTCCTCTCTGC	SLLQNLAVS
	TGCAGAATCTGGCCGTGTCTGTGACA	VTPIQRIVRS
	CCAATCCAGAGGATCGTGCGCAGCG	GENALKIDI
	GCGAGAACGCCCTGAAGATCGACAT	HVIIPYEGLS
	CCACGTGATCATCCCCTACGAGGGCC	ADQMAQIEE
	TGTCCGCCGATCAGATGGCCCAGATC	VFKVVYPVD
	GAGGAGGTGTTCAAGGTGGTGTATCC	DHHFKVILP
	AGTGGACGATCACCACTTCAAAGTGA	YGTLVIDGV
	TCCTGCCCTACGGCACCCTGGTCATC	TPNMLNYFG
	GACGGAGTGACCCCCAACATGCTGA	RPYEGIAVF
	ATTATTTCGGCCGGCCTTACGAGGGC	DGKKITVTG
	ATCGCCGTGTTTGATGGCAAGAAGAT	TLWNGNKII
	CACCGTGACAGGCACCCTGTGGAACG	DERLITPDGS
	GCAATAAGATCATCGACGAGCGGCT	MLFRVTINS
	GATCACACCTGATGGCTCCATGCTGT	SSGHIEGRH
	TCAGAGTGACCATCAACTCCTCCTCT	MLEMGHHH
	GGACACATCGAGGGCCGCCACATGCT	HHHHHHH
	GGAGATGGGCCATCATCACCATCATC	
	ACCACCACCACCACTGA	

350

351

352

353

Bibliography

1. Casanova, J.L., H.C. Su, and C.H.G. Effort, *A Global Effort to Define the Human Genetics of Protective Immunity to SARS-CoV-2 Infection.* Cell, 2020. **181**(6): p. 1194-1199.
2. Hikmet, F., et al., *The protein expression profile of ACE2 in human tissues.* Mol Syst Biol, 2020. **16**(7): p. e9610.
3. Lan, J., et al., *Structure of the SARS-CoV-2 spike receptor-binding domain bound to the ACE2 receptor.* Nature, 2020. **581**(7807): p. 215-220.
4. Vigneshvar, S., et al., *Recent Advances in Biosensor Technology for Potential Applications - An Overview.* Front Bioeng Biotechnol, 2016. **4**: p. 11.
5. Azad, T., A. Tashakor, and S. Hosseinkhani, *Split-luciferase complementary assay: applications, recent developments, and future perspectives.* Anal Bioanal Chem, 2014. **406**(23): p. 5541-60.
6. Azad, T., et al., *A LATS biosensor screen identifies VEGFR as a regulator of the Hippo pathway in angiogenesis.* Nat Commun, 2018. **9**(1): p. 1061.
7. Azad, T., et al., *A gain-of-functional screen identifies the Hippo pathway as a central mediator of receptor tyrosine kinases during tumorigenesis.* Oncogene, 2020. **39**(2): p. 334-355.
8. Nouri, K., et al., *Identification of Celastrol as a Novel YAP-TEAD Inhibitor for Cancer Therapy by High Throughput Screening with Ultrasensitive YAP/TAZ-TEAD Biosensors.* Cancers (Basel), 2019. **11**(10).
9. Nouri, K., et al., *A kinome-wide screen using a NanoLuc LATS luminescent biosensor identifies ALK as a novel regulator of the Hippo pathway in tumorigenesis and immune evasion.* FASEB J, 2019. **33**(11): p. 12487-12499.
10. Yang, X., T. Azad, and K. Nouri, *Hippo Pathway Bioluminescent Biosensor*. 2019, US Patent App. 16/177,691.
11. England, C.G., E.B. Ehlerding, and W. Cai, *NanoLuc: a small luciferase is brightening up the field of bioluminescence.* Bioconjugate chemistry, 2016. **27**(5): p. 1175-1187.
12. Dixon, A.S., et al., *NanoLuc complementation reporter optimized for accurate measurement of protein interactions in cells.* ACS chemical biology, 2016. **11**(2): p. 400-408.
13. Han, D.P., A. Penn-Nicholson, and M.W. Cho, *Identification of critical determinants on ACE2 for SARS-CoV entry and development of a potent entry inhibitor.* Virology, 2006. **350**(1): p. 15-25.
14. Li, W., et al., *Receptor and viral determinants of SARS-coronavirus adaptation to human ACE2.* EMBO J, 2005. **24**(8): p. 1634-43.
15. Li, Q., et al., *The Impact of Mutations in SARS-CoV-2 Spike on Viral Infectivity and Antigenicity.* Cell, 2020. **182**(5): p. 1284-1294 e9.
16. Chen, J., et al., *Mutations strengthened SARS-CoV-2 infectivity.* arXiv preprint arXiv:2005.14669, 2020.
17. Azad, T., et al., *Nanoluciferase complementation-based biosensor reveals the importance of N-linked glycosylation of SARS-CoV-2 Spike for viral entry.* 2020.
18. Hoffmann, M., et al., *SARS-CoV-2 cell entry depends on ACE2 and TMPRSS2 and is blocked by a clinically proven protease inhibitor.* Cell, 2020.
19. Mohandas, S., et al., *Evaluation of the susceptibility of mice & hamsters to SARS-CoV-2 infection.* The Indian Journal of Medical Research, 2020. **151**(5): p. 479.
20. Mohandas, S., et al., *Evaluation of the susceptibility of mice & hamsters to SARS-CoV-2 infection.* Indian J Med Res, 2020. **151**(5): p. 479-482.

21. Brest, P., et al., *Host Polymorphisms May Impact SARS-CoV-2 Infectivity.* Trends Genet, 2020. **36**(11): p. 813-815.
22. Cao, Y., et al., *Comparative genetic analysis of the novel coronavirus (2019-nCoV/SARS-CoV-2) receptor ACE2 in different populations.* Cell Discov, 2020. **6**: p. 11.
23. Starr, T.N., et al., *Deep Mutational Scanning of SARS-CoV-2 Receptor Binding Domain Reveals Constraints on Folding and ACE2 Binding.* Cell, 2020. **182**(5): p. 1295-1310 e20.
24. Tai, W., et al., *Characterization of the receptor-binding domain (RBD) of 2019 novel coronavirus: implication for development of RBD protein as a viral attachment inhibitor and vaccine.* Cell Mol Immunol, 2020. **17**(6): p. 613-620.
25. Lam, T.T., et al., *Identifying SARS-CoV-2-related coronaviruses in Malayan pangolins.* Nature, 2020. **583**(7815): p. 282-285.
26. Zhang, T., Q. Wu, and Z. Zhang, *Probable Pangolin Origin of SARS-CoV-2 Associated with the COVID-19 Outbreak.* Curr Biol, 2020. **30**(7): p. 1346-1351 e2.
27. Liu, P., et al., *Are pangolins the intermediate host of the 2019 novel coronavirus (SARS-CoV-2)?* PLoS Pathog, 2020. **16**(5): p. e1008421.

Figure Legends:

Figure 1. Schematic of SARS-CoV-2 viral entry and the NanoBiT biosensor. (A) Schematic of SARS-CoV-2 viral entry via the interaction between the receptor binding domain (RBD) of the spike glycoprotein and the host cell receptor ACE2. (B) Illustration of the NanoBiT complementation-based biosensor which detects interactions between RBD fused to LgBiT and ACE2 fused to SmBiT.

Figure 2. ACE2 amino acids in 3D structure of the bound RBD and ACE2 and schematic representation of mutations in ACE2. (A) 3D illustration of the overall structure of RBD bound to ACE2. RBD is colored in green, receptor-binding motif (RBM) of RBD is in dark blue, and ACE2 is in dark cyan. (B) Enlarged view of the overall structure depicting ACE2 target mutation sites in stick rendition. Sticks are represented in yellow color. (C-D) ACE2 target mutation sites in stick representation at the contact site of two molecules. Dotted lines connect the mutant AAs to their contacting AAs in RBM. The structure is from PDB: 6M0J based on the information provided in Lan et al. 2020 (E) Illustration of the amino acid changes used to examine ACE2 in this study.

Figure 3. ACE2 mutational analyses with CoV-NanoBiT facilitates delineation of critical host and viral determinants of ACE2-RBD interaction. (A) Immunoblot of SmBiT-ACE2 mutant expression from the cell lysates of transfected HEK293T cells. β-actin and total protein loading are shown as controls. (B-D) Biosensor assay with SmBiT-ACE2 mutants and (B) LgBiT-SARS CoV-2 RBD, (C) LgBiT-SARS CoV-2 Spike S1, or (D) LgBiT- SARS-CoV-1 RBD demonstrating altered binding affinity of various mutants.

Figure 4. Lentiviral pseudovirus infectivity assay of ACE2 mutational analyses reinforces critical host and viral determinants of ACE2-RBD interaction. (A) Schematic of the lentiviral SARS-CoV-2 pseudovirus infectivity assay demonstrating spike-pseudotyped lentiviral attachment to ACE2 host receptor or mutant ACE2 proteins. (B) Lentiviral pseudovirus infectivity assay demonstrating the capacity of each mutant examined to act as a competitive inhibitor for the spike-host ACE2 interaction.

Figure 5. Multiple Sequence Alignment Analysis and SNP Frequency Analysis of ACE2 Mutants. (A) Sequences were reordered based on their binding efficiency to RBD. Only the target mutation sites are shown and the non-target amino acids (AA) has been cut out from the alignment representation. The alignment coloring scheme is based on the chemical properties of each AA (each Human AA is green, the AA from the same chemistry is orange, and AA with different chemistry is red. Except for the last column with three AAs which the number of identical AAs to the human determines the color. WebLogo (http://weblogo.threeplusone.com) representation shows a relative scale of the presence of each AA in each column. (B) dbSNP data on single nucleotide Polymorphism in the ACE2 nucleotide sequence on the target amino acid codons. The frequency of each SNP in different datasets was gathered in the last column. A synonymous mutation (no effect on the protein sequence) is green and missense mutations are red.

Figure 6. (A-F) Visualization of RBD N501 and E484 mutations. (A) overall structure of RBD and ACE2 interaction. (B) the loop structure in RBD containing E484 residue. (C) Predicted structure following E484 residue mutation to lysine which would not significantly change the nature of its interaction in the loop structure of RBD, (D) the N501 residue and its interacting residues in RBM and ACE2. (E) Predictedstructure when the N501 residue mutates to Alanine which would eliminate ACE2 interaction but preserve internal RBM interactions. (F) Predicted structure when the N501 residue mutates to tyrosine which would preserve and slightly boosts internal interactions and introduces an stronger interaction site with ACE2 compared to the wild type residue. (G) ACE2 demonstrating altered binding affinity of various mutants of RBD-LgBiT-mutants.(H) Immunoblot of RBD-LgBiT mutant expression from the cell lysates of transfected HEK293T cells. β-actin and total protein loading are shown as controls. Competition biosensor assay with LgBiT-RBD mutants which maintained any binding capacity pre-incubated with (I) recombinant RBD protein or (J) neutralizing antibody to examine therapeutic implications of various mutants.

Figure 7. Multiple Sequence Alignment Analysis of RBD Mutants. (A) Only the target mutation sites are shown and the non-target amino acids (AA) has been cut out from the alignment representation. The alignment coloring scheme is based on the chemical properties of each AA (each SARS-CoV-2 AA is green, the AA from the same chemistry is orange, and AA with different chemistry is red. WebLogo (http://weblogo.threeplusone.com) representation shows a relative

474 scale of the presence of each AA in each column. (B) Cross species comparison of RBD amino
475 acids in SARS-CoV-2, Pangolin-CoV 2020 and Bat-CoV-RaTG13. Selected mutants are identified
476 by colored boxes. Colored changes indicate RBD AA differences (V445A and F486A and
477 Y505A).

478

479

480

481

482

483

484

485

486

Figure 1

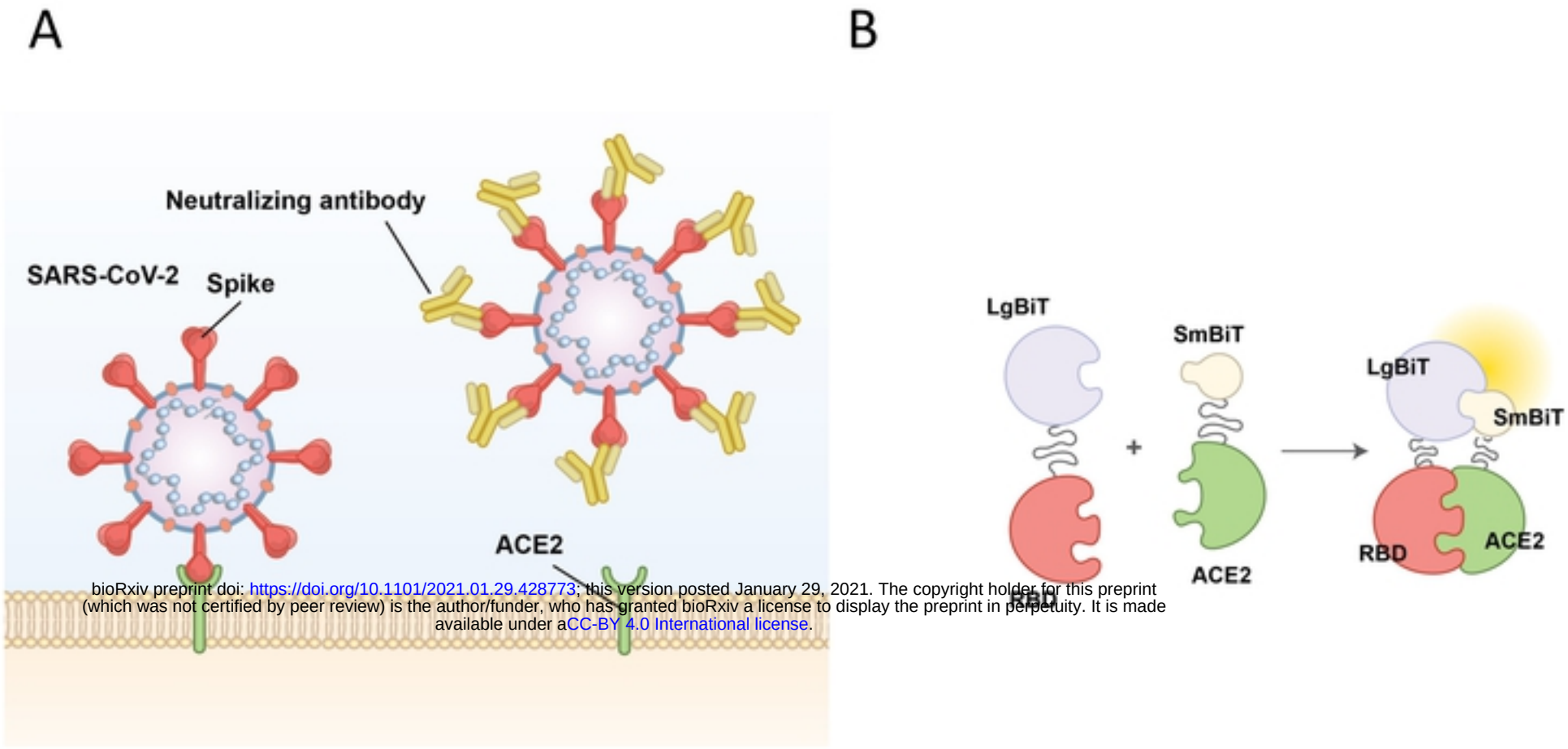

Figure 2

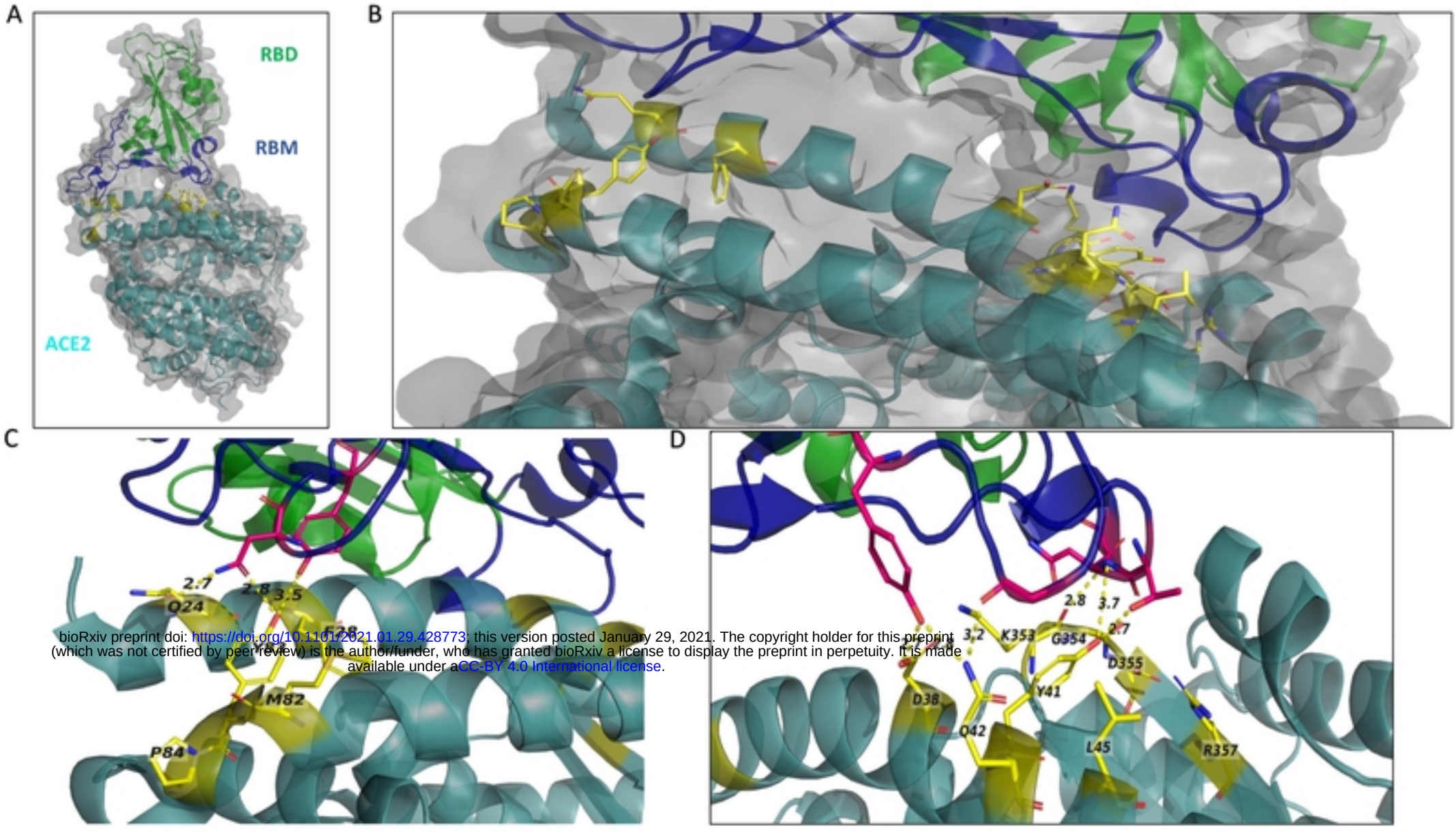

Figure 3

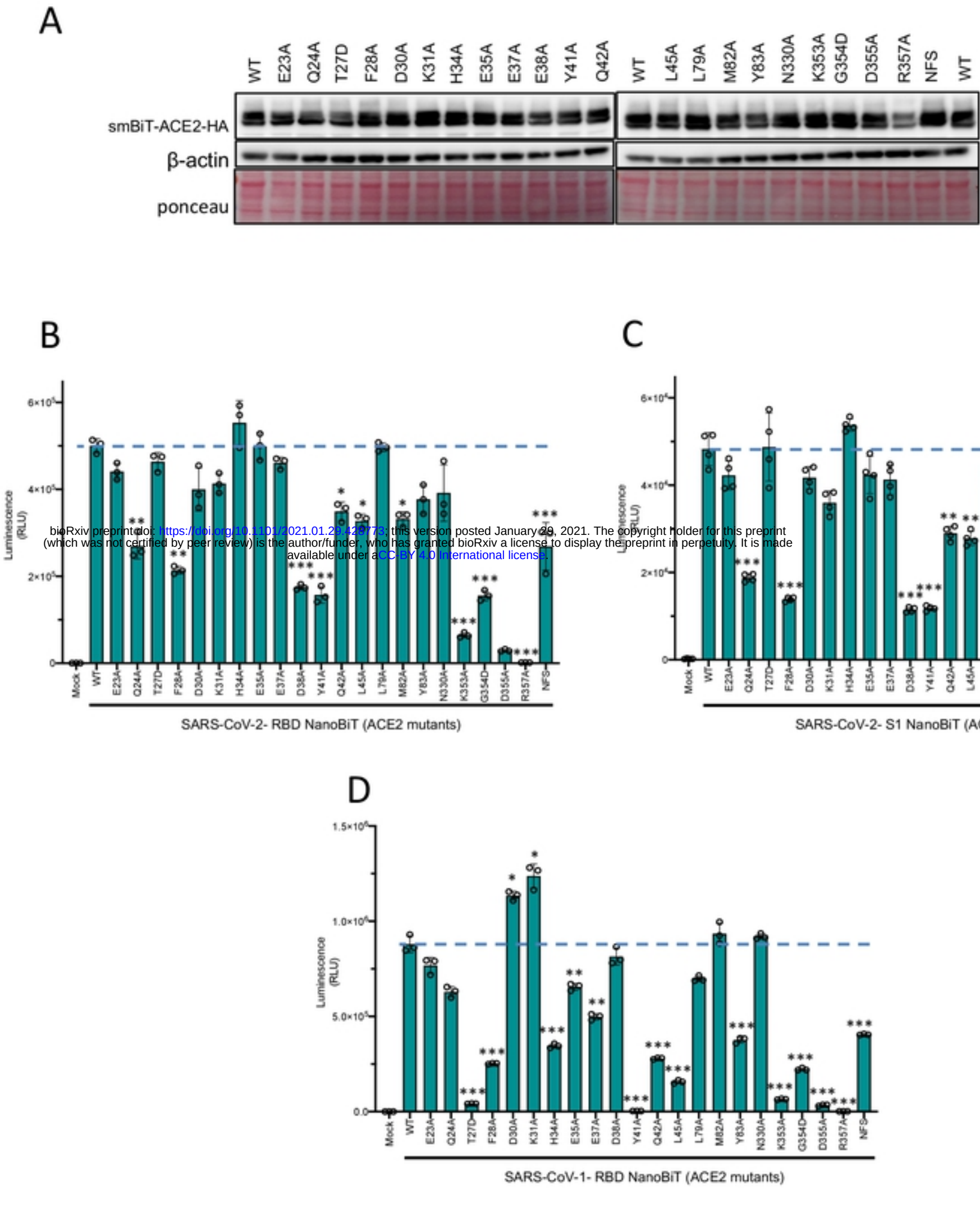

Figure 4

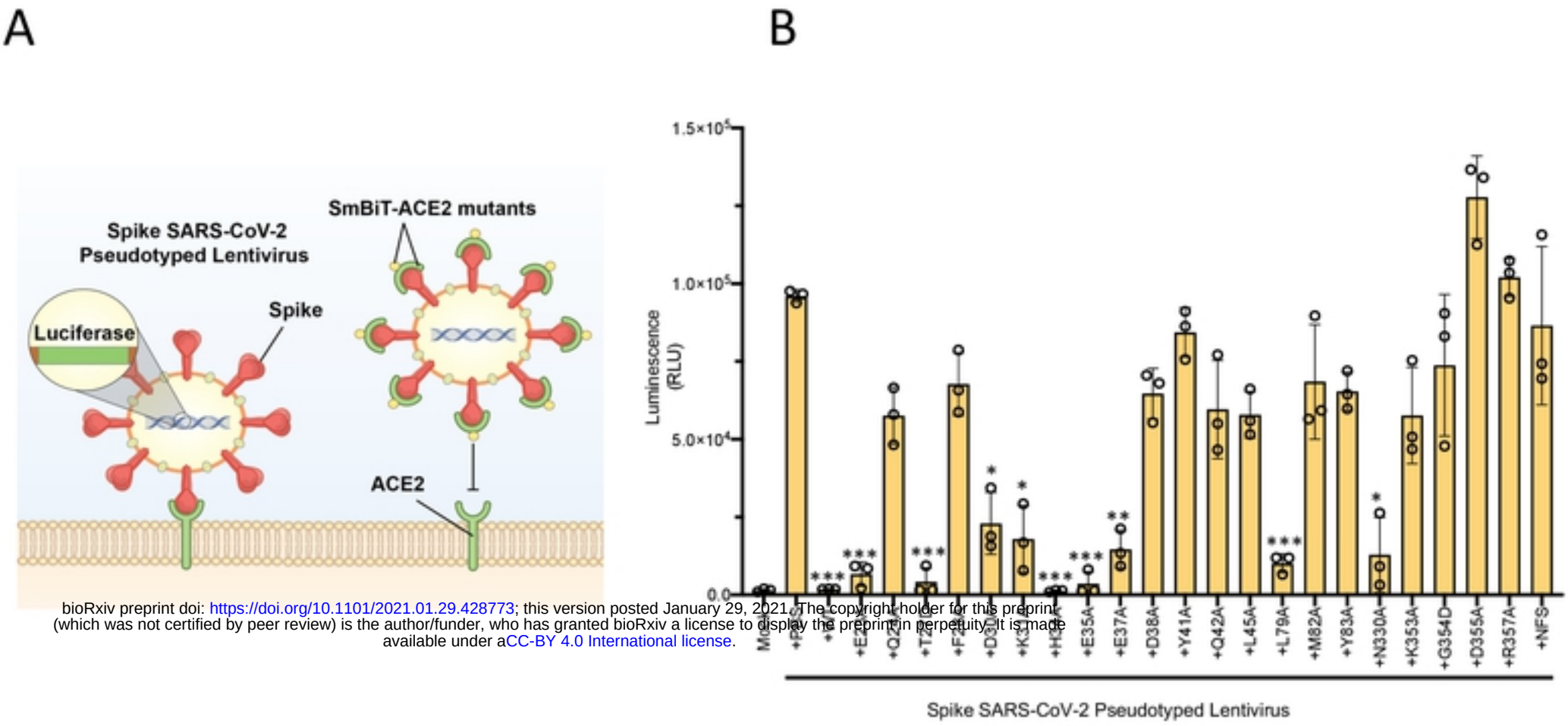

Figure 5

A

Multiple Sequence Alignment			Mutations										
Binomial Name	Common Name	Binding Efficiency	Q24A	F28A	D38A	Y41A	Q42A	L45A	M82A	Y83A	K353A	G354D	D355A	R357A	MYP82-85NFS
Homo sapiens	Human	5	Q	F	D	Y	Q	L	M	Y	K	G	D	R	MYP
Pan troglodytes	Chimpanzee	5	Q	F	D	Y	Q	L	M	Y	K	G	D	R	MYP
Tursiops truncatus	Dolphin	4	R	F	D	Y	Q	L	T	Y	K	G	D	R	TYP
Cricetulus griseus	Hamster	4	Q	F	D	Y	Q	L	N	Y	K	G	D	R	NYS
Ovis aries	Sheep	3	Q	F	D	Y	Q	L	T	Y	K	G	D	R	TYS
Felis catus	Cat	3	L	F	E	Y	Q	L	T	Y	K	G	D	R	TYP
Canis lupus familiaris	Dog	2	L	F	E	Y	Q	L	T	Y	K	G	D	R	TYP
Equus caballus	Horse	2	L	F	E	H	Q	L	T	Y	K	G	D	R	TYP
Sus scrofa	Pig	2	L	F	D	Y	Q	L	T	Y	K	G	D	R	TYP
Mus musculus	Mouse	1	N	F	D	Y	Q	L	S	F	H	G	D	R	SFS
Rattus norvegicus	Rat	1	K	F	D	Y	Q	L	N	F	H	G	D	R	NFS
		WebLogo													

B

Mutations	dbSNP id	Frequency	dbSNP allele	Protein Residue	Codon position	AA position	
Q24A	-	-	-	-	-	-	-
F28A	-	-	-	-	-	-	-
D38A	-	-	-	-	-	-	-
Y41A	-	-	-	-	-	-	-
Q42A	-	-	-	-	-	-	-
L45A	-	-	-	-	-	-	-
NFS (MYP)	rs766996587	reference	G	Met [M]	3	82	T=0.000011 (2/182758, GnomAD_exome) T=0.000048 (6/125568, TOPMED) T=0.00001 (1/87698, ExAC) T=0.00014 (3/22011, GnomAD) T=0.0000 (0/2188, ALFA Project)
		missense	T	Ile [I]	3	82	
		missense	A	Ile [I]	3	82	
	rs759134032	reference	C	Pro [P]	1	84	T=0.000005 (1/182792, GnomAD_exome) T=0.00001 (1/87705, ExAC)
		missense	A	Thr [T]	1	84	
K353A	-	-	-	-	-	-	-
G354D	rs200909433	reference	C	Gly [G]	3	354	A=0.000016 (2/125568, TOPMED)
		synonymous	T	Gly [G]	3	354	
D355A	rs961360700	reference	G	Asp [D]	1	355	T=0.000012 (2/170310, GnomAD_exome) T=0.0001 (1/8986, ALFA Project)
		missense	A	Asn [N]	1	355	
R357A	-	-	-	-	-	-	-

Figure 6

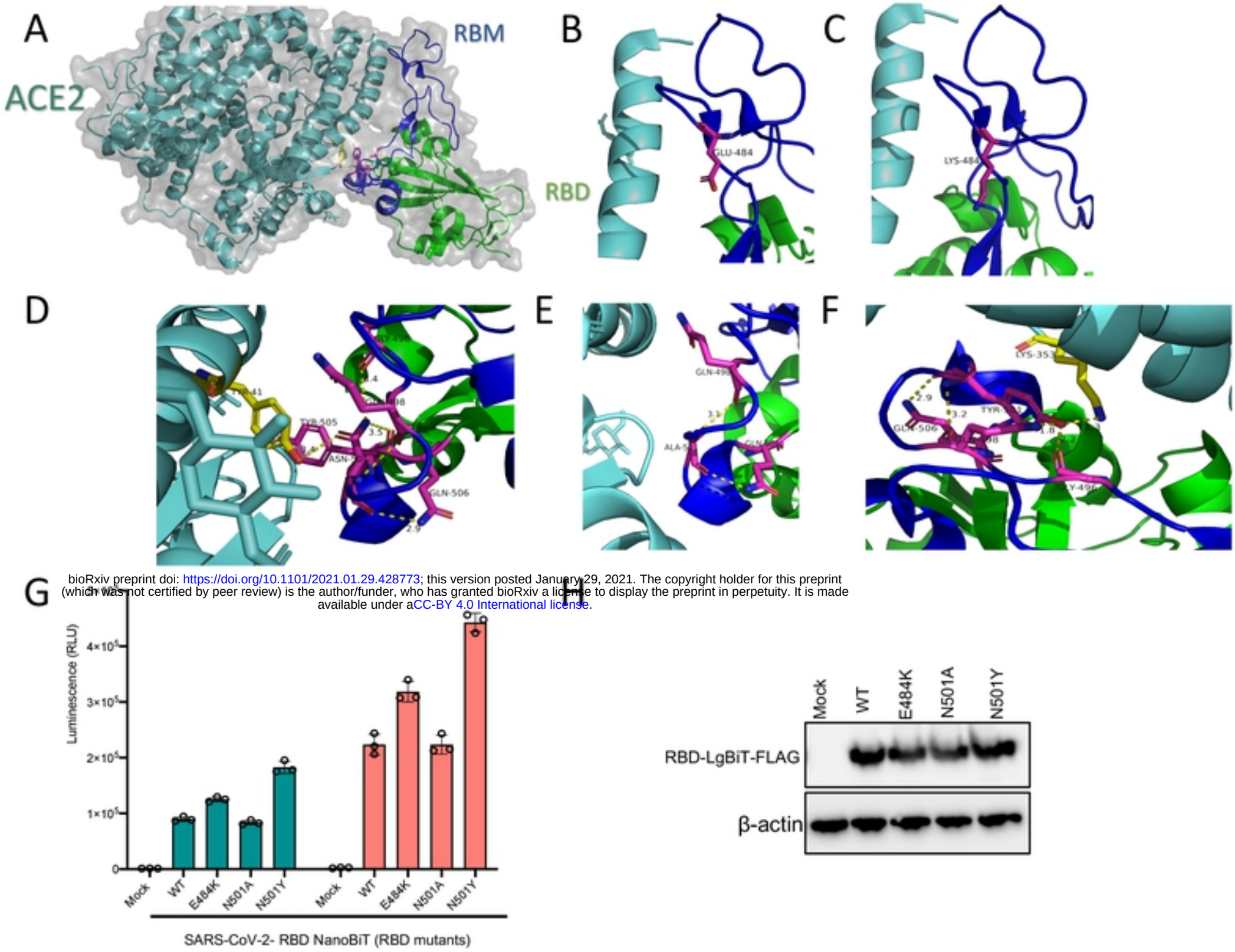

Figure 7

A

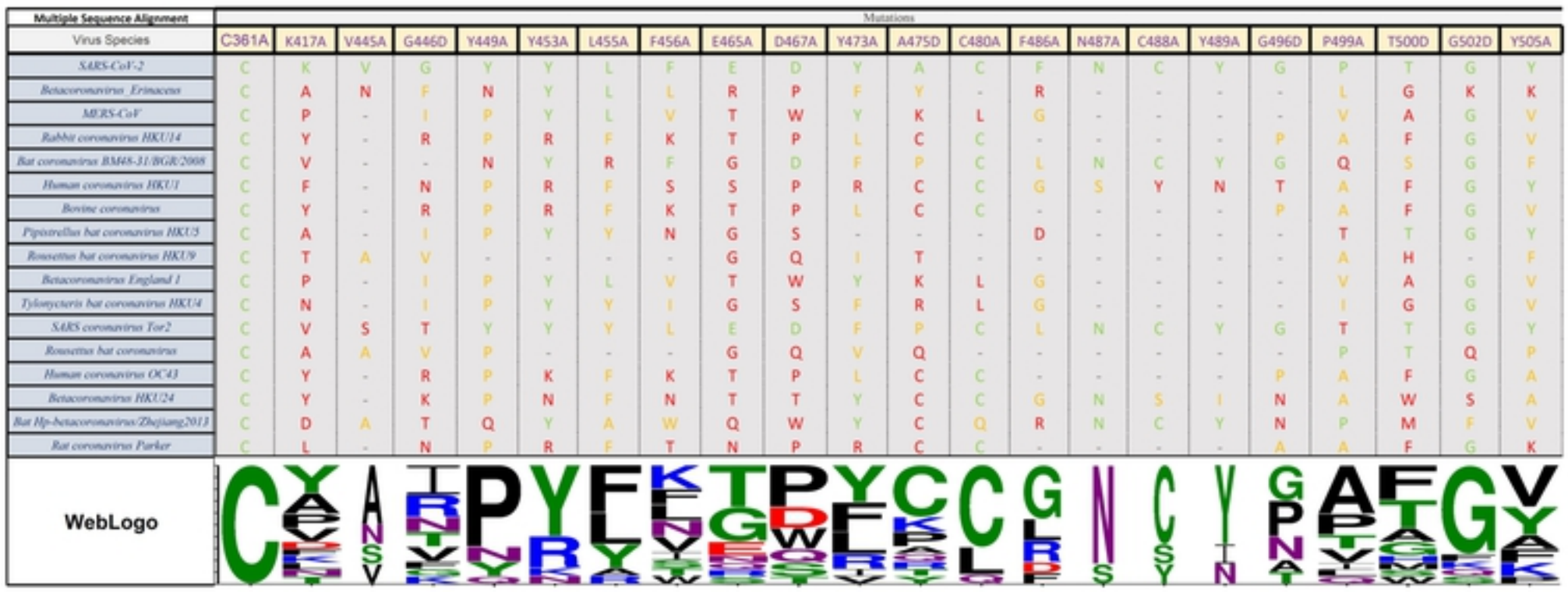

B